Contribution from the Laboratoire de Photochimie Générale, ERA du CNRS No. 386, ENSCM, 68093 Mulhouse Cedex, France, Institut de Physique Nucléaire (et IN2P3), Université de Lyon-I, 69622 Villeurbanne Cedex, France, Laboratoire de Chimie Inorganique Moléculaire, Université d'Aix Marseille St Jérôme, 13397 Marseille Cedex 13, France, and Department of Chemistry and Chemical Engineering and the Saskatchewan Accelerator Laboratory, University of Saskatchewan, Saskatoon, Saskatchewan S7N 0W0, Canada

Xα Method as a Tool for Structure Elucidation of Short-Lived Transients Generated by Pulse Radiolysis or Flash Photolysis. 1. Reductive Reactions of $PtCl_6^{2-}$

A. GOURSOT,† H. CHERMETTE,*‡ E. PENIGAULT,† M. CHANON,§ and W. L. WALTZ‖

Received February 2, 1984

Relativistic MS–Xα calculations have been performed on $Pt^{III}Cl_6^{3-}$, $PtCl_5^{2-}$, and $PtCl_4^-$ complexes, which have been proposed as models for short-lived transients generated by pulse radiolysis or flash photolysis of $Pt^{IV}Cl_6^{2-}$. The $Pt^{III}Cl_6^{3-}$ complex with O_h symmetry displays a delocalized $3e_g$ HOMO corresponding to strong antibonding interactions of the Pt $5d\sigma$ (d_{z^2}, $d_{x^2-y^2}$) orbitals with the Cl 3s and $3p\sigma$ orbitals. The comparison with $Pt^{IV}Cl_6^{2-}$ shows that, for this complex, the dissociative activation induced by electron transfer mainly lies in the population of a σ antibonding orbital. This conclusion is confirmed by a detailed analysis of isodensity contours. The simulation of a Jahn–Teller distortion toward a D_{4h} symmetry for $PtCl_6^{3-}$ shows the great stability of the levels involving the equatorial chlorine orbitals and underlines the significant red shift of the LMCT transitions when the axial Pt–Cl bonds are elongated. The Xα method suggests that the simple representation of Jahn–Teller-distorted $Pt^{III}Cl_6^{3-}$ where a square complex is slightly disturbed by two axial Cl^- ligands is a sound one. In $Pt^{III}Cl_4^-$ the singly occupied HOMO is $2b_{2g}$ (π-antibonding interactions of the Pt $5d_{xy}$ and Cl $3p\pi$ orbitals) but the net charge on Pt is not very different from the one calculated for the most distorted $Pt^{III}Cl_6^{3-}$ structure. $PtCl_5^{2-}$ (D_{3h}) has a 5e′ HOMO corresponding to mixed σ- and π-antibonding interactions between the Pt $5d_{x^2-y^2}$ and $5d_{xy}$ orbitals with the $3p\sigma$ and $3p\pi$ orbitals of the equatorial ligands. For all of these complexes, the most intense UV absorption bands correspond to LMCT: for $PtCl_6^{3-}$ (O_h), they are expected at 228, 212, and 175 nm; for $PtCl_4^-$ (D_{4h}), two bands at 410 and 620 nm are calculated; for $PtCl_5^{2-}$ (D_{3h}), the most intense bands should be observed at 264 and 232 nm. The comparison of these theoretical values with experimental results suggests the following: (a) The common species, generated by pulse radiolysis and flash photolysis of $Pt^{IV}Cl_6^{2-}$, is best described as being $Pt^{III}Cl_4^-$ (D_{4h}), although the possibility of weakly coordinating apical positions cannot be ruled out. (b) For $Pt^{IV}Cl_6^{2-}$, the direct homolysis of the Pt^{IV}–Cl bond seems to be the primary event on photoexcitation rather than the indirect homolysis (induced by intermolecular electron transfer in the excited state). (c) The simulation of $PtCl_5^{2-}$ with the framework of C_{4v} and D_{3h} models as postulated in previous pulse radiolysis work does not fit with experimental results. The Xα method seems to be a useful complementary tool in elucidating the structure of transients generated by flash photolysis and pulse radiolysis.

Introduction

The importance of the chemistry of platinum and its coordination compounds is widely recognized from both applied and fundamental viewpoints.[1,2] Furthermore, interest in these systems now goes well beyond the more traditional boundaries of chemistry, with the recent and exciting developments in the use of platinum complexes in cancer chemotherapy as one notable example.[3] In contrast to the extensive experimental efforts directed at platinum coordination compounds, there is, in a relative sense, a paucity of theoretical treatments.[4] One of the main reasons for this situation appears to be intrinsic difficulties in dealing with these systems by elaborate theoretical methods.[5] This paper is in general addressed to this aspect through the application of the Xα method, but there are also specific facets of concern. A major one is associated with the increasing recognition that monomeric and polymeric platinum species where the metal center(s) is formally in the unusual oxidation state of III can play an important role in a wide variety of chemical processes.[11b-e] At least for the monomeric forms, their very transitory existence presents a formidable challenge in terms of not only their detection but also, more importantly, the elucidation of their structures in correlation with reactivity.

In this context, our interest in the adoption of a theoretical approach was motivated initially by the possibility of rationalizing the light-initiated reaction of radiochloride exchange[6]

$$Pt^{IV}Cl_6^{2-} + 6{}^*Cl \xrightarrow{h\nu} Pt^{IV}{}^*Cl_6^{2-} + 6Cl^-$$

within the electron-transfer catalysis scheme[7a-c] (more commonly designated as SRNI[7d] or electron-transfer-induced chain reaction[7e,f]). One of us has also proposed for this reaction a type of mechanism that is not generally considered in inorganic photochemistry at this time although it has recently and independently been proposed for organometallic substrates.[8] The main and novel aspect of this mechanism rests in the proposition that the role of light rather than leading to "direct homolysis of the Pt^{IV}–Cl bond" (Scheme I) could be to generate "indirect homolysis induced by photoelectron transfer from an external nucleophile to a highly oxidizing[9] excited state

† ENSCM.
‡ Université de Lyon-I.
§ Université d'Aix Marseille St Jérôme.
‖ University of Saskatchewan.

(1) (a) J. S. Griffith, "The Chemistry of the Rarer Platinum Metals", Wiley Interscience, New York, 1968; (b) U. Belluco, "Organometallic and Coordination Chemistry of Platinum", Academic Press, London, 1974.
(2) See *Platinum Met. Rev.* for pertinent articles.
(3) (a) B. Rosenberg, L. Van Camp, J. E. Troska, and V. H. Mansour, *Nature (London)*, **222**, 385 (1969); (b) B. Rosenberg, *Platinum Met. Rev.* **15**, 42–51 (1971); (c) A. J. Thomson, R. J. Williams, and S. Reslova, *Struct. Bonding (Berlin)*, **11**, 1 (1972); (d) M. J. Cleare and J. D. Hoeschele, *Platinum Met. Rev.*, **17**, 2–13 (1973); (e) B. Rosenberg, *Naturwissenschaften*, **60**, 399–406 (1973).
(4) (a) R. P. Messmer, *Int. J. Quantum Chem., Symp.*, No. 7, 371 (1973); (b) R. P. Messmer, L. V. Interrante, and K. H. Johnson, *J. Am. Chem. Soc.*, **96**, 3847 (1974); (c) N. Rösch, R. P. Messmer, and K. H. Johnson, *J. Am. Chem. Soc.*, **96**, 3855 (1974); (d) M. Barber, J. D. Clark, and A. Hinchcliffe, *J. Mol. Struct.*, **57**, 305 (1979); (e) M. Barber, J. D. Clark, and A. Hinchcliffe, *J. Mol. Struct.*, **57**, 169 (1979).
(5) J. H. Jaffri, J. Logan, and M. D. Newton, *Isr. J. Chem.*, **19**, 340–350 (1980).
(6) R. L. Rich and H. Taube, *J. Am. Chem. Soc.*, **76**, 2608 (1954).
(7) (a) M. Chanon and M. L. Tobe, *Angew. Chem., Int. Ed. Engl.*, **21**, 1 (1982); (b) M. Chanon, *Bull. Soc. Chim. Fr.*, 197 (1982); (c) M. Julliard and M. Chanon, *Chem. Rev.*, **83**, 425 (1983); (d) J. F. Bunnet, *Acc. Chem. Res.*, **11**, 413 (1978); (e) N. Kornblum, R. E. Michel, and R. C. Kerber, *J. Am. Chem. Soc.*, **88**, 5662 (1966); (f) G. A. Russel and W. C. Danen, *J. Am. Chem. Soc.*, **88**, 5663 (1966).
(8) D. P. Summers, J. C. Luong, and M. S. Wrighton, *J. Am. Chem. Soc.*, **103**, 5238 (1981).
(9) (a) L. E. Cox, D. G. Peters, and E. L. Wehry, *J. Inorg. Nucl. Chem.*, **34**, 297 (1972); (b) G. A. Shagisultanova, A. A. Karaban, R. M. Orisheva, and S. P. Gorbuna, in "Prevrashch Kompleks Soedin Diestviem Sveta Radiats Temp", Lazerko, G. A., Ed., Izd. Beloruss Gos University, Minsk, USSR, 1973, pp 45–53; (c) A. V. Loginov, V. A. Yakoslov, and G. A. Shagisultanova, *Koord. Khim.*, **5**, 733 (1979).

0020-1669/84/1323-3618$01.50/0

of Pt^{IV}, followed by easy cleavage of a labile Pt^{III} complex so created" (Scheme II).

Scheme I

$$Pt^{IV}Cl_6^{2-} \xrightarrow{h\nu} Pt^{IV}Cl_6^{2-*} \rightarrow Pt^{III}Cl_5^{3-} + Cl\cdot$$

Scheme II

$$Pt^{IV}Cl_6^{2-} \xrightarrow{h\nu} Pt^{IV}Cl_6^{2-*} \xrightarrow{Cl^-} Pt^{III}Cl_6^{3-} + Cl\cdot$$

$$Pt^{III}Cl_6^{3-} \rightarrow Pt^{III}Cl_5^{2-} + Cl^-$$

The central characters in these schemes are platinum(III) species, and within recent years, the application of the fast reaction techniques of flash/laser photolysis has provided the means to detect and characterize the reactions of a number of short-lived Pt^{III} halide and amine systems.[10,11] While the results clearly point to the occurrence of different structural types, and they have provided the grounds for reasonable suggestions as to the possible limiting structural forms, there are conflicting proposals. A tool to aid in structure characterizations would therefore be welcomed specifically with regard to Pt^{III} intermediates and more generally in the rapidly expanding area focusing on short-lived inorganic complexes[12] and frequently involving pulse radiolysis and flash photolysis methods.[13,14] The present report therefore is aimed at two objectives: *the first is to provide a consistent theoretical treatment of some aspects of platinum chemistry*, through the consideration of some chloro complexes, and *the second and closely connected one is to discern to what extent the Xα method*[15] *can be used* as an efficient and complementary means in the structural elucidation of short-lived inorganic species.

It is worth underlining that the simple use of symmetry arguments and energy level diagrams derived from ligand field theory already provides helpful indications about the nature of the ground and excited states of the proposed structures. But it remains that the true characterization of a specific transient must be through the agreement between the calculated CT spectrum and the experimentally observed one. This agreement is directly related to the suitable description of the relative positions of the ground state and the possible CT excited states. This problem, principally for heavy-metal complexes, could be resolved neither by ligand field theory nor by a simple MO approach. The Xα method, including relativistic corrections, has been chosen for this reason. Moreover, we have first verified the validity of the Xα description of the CT excited state in studying the stable and well-characterized $Pt^{IV}Cl_6^{2-}$[16] and $Pt^{II}Cl_4^{2-}$[17] complexes. The next step has been the treatment of the "between case" of Pt^{III} complexes exhibiting various geometries and coordination numbers with the aim of simulating the various structures proposed in the literature for these transients. The results described herein strongly suggest that the Xα method can be a useful complementary method of structure elucidation for transients observed by fast spectroscopies.

Statement of the Problem

The transient spectrum arising on pulse radiolysis of an aqueous solution of $K_2[PtCl_6]$ exhibits an absorption peak at 410 nm, which develops over a period of about 20 μs after the pulse.[11a] This absorption maximum is assigned to a transitory Pt(III) complex:

$$e_{aq}^- + Pt(IV) \rightarrow Pt(III)$$

However, from the delay in its development relative to the disappearance of e_{aq}^-, this species is probably not the initial product.[11a] The same transient, absorbing at 410 nm, is also detected on flash photolysis of $Na_2[PtCl_6]$, in the presence of Cl^- anions,[10c] and these features imply the sequence of events

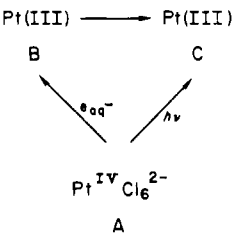

where C is the transient absorbing at 410 nm and B the assumed initial product in the pulse radiolysis experiment, for which the spectrum could not be obtained.[11a] Wright and Laurence[10c] have proposed that C may be $PtCl_4^-$, while Adams and co-workers[11a] suggested that A is initially reduced to $Pt^{III}Cl_6^{3-}$ (B), which then dissociates into the five-coordinate complex $Pt^{III}Cl_5^{2-}$ (C). Moreover, they assign to C a trigonal-bipyramidal structure. Previous SCF–Xα results on $PtCl_6^{2-}$[16] have shown that the calculated ionization and absorption spectra of this complex are in good agreement with experiment, particularly so for LMCT type transitions, which involve the greatest orbital relaxation and are used experimentally to characterize the transient absorptions.

Our strategy is thus to investigate the electronic structure and to calculate the absorption spectra of the species that have been postulated for the transients B and C and eventually extend this to deformed geometries: For B, we examine $PtCl_6^{3-}$ with equal bond lengths (O_h) or with elongated axial Pt–Cl distances (D_{4h}) to account for the Jahn–Teller deformation. The use of various standard elongations allows us to analyze the influence of the axial bond lengthening upon the CT absorption spectrum. For C, we examine $PtCl_5^{2-}$ (D_{3h} and C_{4v}) and $PtCl_4^-$ (D_{4h}). Only the calculated absorption spectrum of $PtCl_5^{2-}$ (C_{4v}) is reported; the Xα electronic structure of this model will be presented elsewhere.[17]

The calculated absorption spectra of these models are then compared with the experimental data.

Computational Details

The Pt–Cl bond lengths of $PtCl_6^{2-}$ and $PtCl_4^{2-}$ have been experimentally determined to be nearly equal to 2.32 Å.[18,19] We have thus adopted this value for transient models with undeformed structures.

(10) (a) S. A. Penkett and A. W. Adamson, *J. Am. Chem. Soc.*, **87**, 2514 (1965); (b) P. D. Fleischauer, Ph.D Dissertation, University of Southern California, Los Angeles, CA, 1968; (c) R. C. Wright and G. S. Laurence, *J. Chem. Soc., Chem. Commun.*, 132 (1972).
(11) (a) G. E. Adams, R. B. Broszkiewicz, and B. D. Michael, *Trans. Faraday Soc.*, **64**, 1256 (1968); (b) D. K. Storer, W. L. Waltz, J. C. Brodovitch, and R. L. Eager, *Int. J. Radiat. Phys. Chem.*, **7**, 693 (1975); (c) J. C. Brodovitch, D. K. Storer, W. L. Waltz, and R. L. Eager, *Int. J. Radiat. Phys. Chem.*, **8**, 465 (1976); (d) H. M. Kahn, W. L. Waltz, R. J. Woods, and J. Lilie, *Can. J. Chem.*, **59**, 3319 (1981); (e) H. M. Kahn, W. L. Waltz, J. Lilie, and R. J. Woods, *Inorg. Chem.*, **21**, 1489–1497 (1982).
(12) G. V. Buxton and R. M. Sellers, *Coord. Chem. Rev.*, **22**, 195 (1977).
(13) M. X. Matheson, *IEEE Trans. Nucl. Sci.*, **NS-26**, 1739–43 (1979); M. S. Matheson and L. M. Dorfman, "Pulse Radiolysis", American Chemical Society, Washington, DC, 1969.
(14) G. Porter and M. A. West, *Tech. Chem. (N.Y.)* **6**, 367 (1974).
(15) K. H. Johnson, *Adv. Quantum Chem.*, **7**, 143 (1973); H. Chermette, *FCTL, Folia Chim. Theor. Lat.*, **9**, 47 (1981); R. Rosch, "Electrons in Finite and Infinite Structures", Phariseau, P., Ed., Plenum Press, New York 1977.
(16) A. Goursot, E. Penigault, H. Chermette, *Chem. Phys. Lett.*, **97**, 215 (1983).
(17) (a) A. Goursot and H. Chermette, *Can. J. Chem.*, in press; (b) A. Goursot, H. Chermette, M. Chanon, and W. L. Waltz, to be submitted for publication.
(18) R. J. Williams, D. R. Dillin, and W. O. Milligan, *Acta Crystallogr. Sect. B: Struct. Crystallogr. Cryst. Chem.*, **B29**, 1369 (1973).
(19) R. G. Dickinson, *J. Am. Chem. Soc.*, **44**, 2404 (1922).

Table I. Electronic Energy Levels[a] and Percent Charge Distribution of $PtCl_6^{3-}$

MO	energy, Ry	Pt						Cl			inter sphere	outer sphere
		s	p_z	$p_{x,y}$	$d\pi$	$d\sigma$	f	s	$p\sigma$	$p\pi$		
$3e_g$	−0.105					52		4	29		8	7
$2t_{2g}$	−0.346				68					21	10	1
$1t_{1g}$	−0.445									90	9	1
$3t_{1u}$	−0.480		2				2		38	47	8	3
$1t_{2u}$	−0.491						1			86	12	1
$2t_{1u}$	−0.577		1	5				1	48	33	10	2
$1t_{2g}$	−0.622				25					59	16	
$2e_g$	−0.684					41		1	57			1
$2a_{1g}$	−0.705	20						4	71		4	1
$1t_{1u}$	−1.363			2				95			3	
$1e_g$	−1.365					5		94			1	
$1a_{1g}$	−1.414	6						89	1		4	

[a] The highest occupied level is $3e_g$, which accommodates 1 electron.

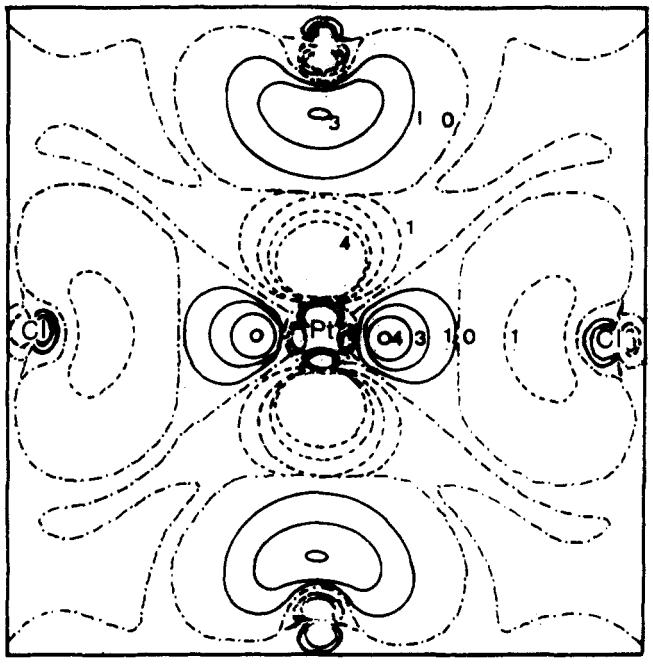

Figure 1. Wave function contours of the $3e_g$ HOMO of $PtCl_6^{3-}$ plotted in the $z0x$ plane ($-z$ axis collinear with the C_4 axis). Contour labels 0–5 indicate values equal to 0, 0.050, 0.100, 0.150, 0.200, and 0.250 $(e/bohr^3)^{1/2}$, respectively, and are the same for all wave function contour plots. Positive wave function contours are indicated by solid lines, negative contours by dotted lines, and zero contours by dashed lines.

For calculations with elongated axial Pt–Cl bond distances, standard elongations of 0.2, 0.4, and 1 au have been used for $PtCl_6^{3-}$ and 0.4 au for $PtCl_5^{2-}$ (D_{3h}).

The radii of platinum and chlorine atomic spheres are the same as those used in the $PtCl_6^{2-}$ case.[16]

$$R(Pt) = 2.561\,73 \text{ au} \qquad R(Cl) = 2.706\,07 \text{ au}$$

An externally tangent outer sphere is used in each case. It also serves as a "Watson sphere"[20] on which a positive charge 3+ ($PtCl_6^{3-}$), 2+ ($PtCl_5^{2-}$), or 1+ ($PtCl_4^-$) is distributed to simulate the environment of the complex anion.

The values of atomic exchange parameters α for Pt (0.693 06) and for Cl (0.723 25) are taken from the compilation of Schwarz.[21] Weighted averages of the atomic values are chosen for the interatomic and extramolecular regions (0.718 94, 0.718 22, and 0.717 21 for $PtCl_6^{3-}$, $PtCl_5^{2-}$, and $PtCl_4^-$, respectively).

In the solution of the secular equations, spherical harmonics up to $l = 4$ are included in the platinum sphere and extramolecular region and up to $l = 1$ in the chlorine spheres.

The transition-state method[22] is used for the calculations of the excitation energies, which have been determined with spin polarization.

Table II. Pt and Cl Charge Distributions (in electrons) for $PtCl_6^{3-}$ in Connection with $Pt-Cl_{ax}$ Elongations

	without elongation	with 0.4-au elongation	with 1-au elongation
s	0.52	0.49	0.50
p	0.60	0.52	0.52
$d\pi$	5.58	5.58	5.58
d_{xy}	1.86	1.86	1.86
$d_{xz,yz}$	3.72	3.72	3.72
$d\sigma$	2.36	2.36	2.31
d_{z^2}	1.18	1.42	1.35
$d_{x^2-y^2}$	1.18	0.94	0.96
f	0.18	0.12	0.06
Cl_{eq}			
s	1.96	1.95	1.95
$p\sigma$	1.69	1.66	1.65
$p\pi$	3.97	3.98	3.98
Cl_{ax}			
s	1.96	2.00	2.00
$p\sigma$	1.69	1.79	1.88
$p\pi$	3.97	3.98	3.98
Pt net charge	0.76+	0.93+	1.03+
Cl_{eq} net charge	0.62−	0.59−	0.58−
Cl_{ax} net charge	0.62−	0.77−	0.86−

Electronic Structure of the Transient Models

(1) $Pt^{III}Cl_6^{3-}$. The calculated valence levels of the d^7 $PtCl_6^{3-}$ complex with equal Pt–Cl bond lengths (O_h symmetry) are reported in Table I (spin-restricted case).

The ground state is ^2E_g for the O_h case and $^2A_{1g}$ for the D_{4h} structures. The highest occupied molecular orbital (HOMO) is the singly occupied $3e_g$ MO. As illustrated in Figure 1, it corresponds to strong antibonding interactions of the Pt $5d\sigma$ (d_{z^2}, $d_{x^2-y^2}$) orbitals with the Cl 3s and $3p\sigma$ orbitals. The HOMO exhibits an important delocalization of the unpaired electron since its metal character only amounts to 52% with the intersphere charge being fully attributed to the ligands.[16,23,24] The related bonding MO is $2e_g$, which provides along with $2a_{1g}$ most of the σ-bonding interactions. The metal–ligand π interactions occur through $1t_{2g}$ and $2t_{2g}$ and are respectively bonding and antibonding MOs.

The comparison between the electronic structures of $Pt^{IV}Cl_6^{2-}$[16] and $Pt^{III}Cl_6^{3-}$ shows a significant reduction of the π-electron delocalization for the latter complex. The same evolution, although less pronounced, is observed for the metal

(20) R. E. Watson, *Phys. Rev.*, **111**, 1108 (1958).
(21) (a) K. Schwarz, *Phys. Rev. B: Solid State*, **B5**, 2466 (1972); (b) K. Schwarz, *Theor. Chim. Acta*, **34**, 225 (1974).
(22) J. C. Slater, *Adv. Quantum Chem.*, **6**, 1 (1972).
(23) J. Weber, A. Goursot, E. Penigault, J. H. Ammeter, and J. Bachmann, *J. Am. Chem. Soc.*, **104**, 1491 (1982).
(24) A. Goursot, H. Chermette, and C. Daul, *Inorg. Chem.*, **23**, 305 (1984).

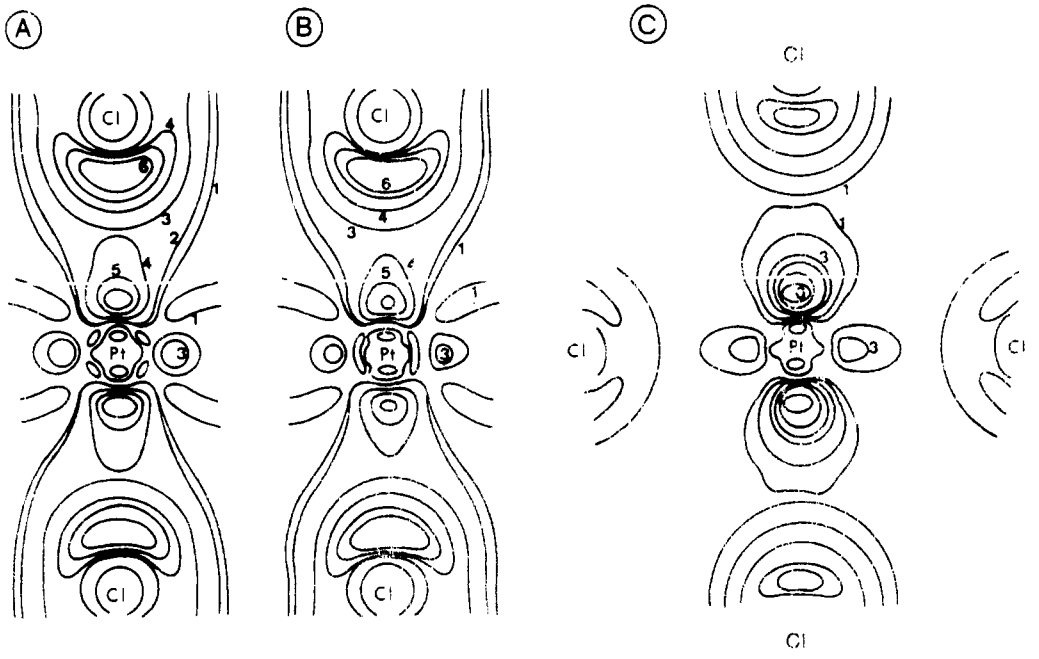

Figure 2. Total σ electronic isodensity contours, plotted in the $z0x$ plane: (A) $PtCl_6^{2-}$ (O_h); (B) $PtCl_6^{3-}$ (O_h); (C) $PtCl_6^{3-}$ (D_{4h}, with 1-au-elongated Pt–Cl_{ax} bonds). Contour values of 1–6 are equal to 0.006, 0.030, 0.042, 0.090, 0.150, and 0.210 e/bohr^3, respectively, and are the same for all the total σ electronic isodensity contours.

5dσ–ligand 3pσ interactions in the $2e_g$ and $3e_g$ MOs. In fact, if the Pt 5f, 6s, 6p and Cl 3s contributions to the MOs remain nearly unchanged, the participation of the Pt 5d and Cl 3p orbitals undergoes substantial modifications. Formally, *the additional electron in $3e_g$ would be attributed half to the metal and half to the ligands, if all other MOs remained unchanged.* However, an important electronic redistribution occurs in the $PtCl_6^{3-}$ MOs, which involves only a small increase (0.2 e) in the Pt charge, while the chlorine 3pσ orbitals recover the major part (80%) of the additional electron. The detailed population analysis from non-spin-polarized results is given in Table II.

In fact, the prevailing factor in the σ-electronic interactions of $PtCl_6^{3-}$ is the population of the σ-antibonding MO $3e_g$, which weakens the metal–ligand σ-bonding framework. To visualize the evolution of the σ-electronic interactions from $PtCl_6^{2-}$, it is convenient to plot the sum of electronic densities, relative to all the populated σ MOs, through isodensity contours (Figure 2). The examination of this figure shows no observable difference between parts A and B in the spherical region surrounding the chlorines: on the contrary, contours 4, 5, and 6 near the metal delineate a far smaller region in part B than in part A. This reduction in electron density between the Pt and Cl nuclei increases the repulsion between them, leading these atoms to move apart. The naive picture of electron-transfer activation toward dissociation (population of an antibonding MO[7a]) is therefore confirmed and made more precise by this more elaborate model.

This is to be related to the observation that $5d^7$ compounds are quite rare in the Pt group. As can also be seen from ESR experiments on d^7 ions in host lattices,[25] a Jahn–Teller effect is implied in connection with a tetragonal distortion of the initial octahedron. To consider this aspect, we have investigated the evolution of the electronic structure of $PtCl_6^{3-}$ through a progressive distortion of the octahedron: this distortion was performed along the z axis, by successively increasing the Pt–Cl_{ax} bond lengths by 0.2, 0.4, and 1 au (0.11, 0.21, and 0.53 Å-, respectively). The initial O_h symmetry is thus lowered to D_{4h}, with the C_4 axis collinear with the z axis.

The evolution of the upper valence energy levels and their metal charge contribution, with respect to the Pt–Cl_{ax} elongation, is illustrated in Figure 3. Of note is that the $O_h \rightarrow D_{4h}$ descent in symmetry splits the e_g dσ levels into a_{1g} (d_{z^2}) and b_{1g} ($d_{x^2-y^2}$) and the t_{2g} dπ levels into b_{2g} (d_{xy}) and e_g (d_{xz}, d_{yz}). Similarly the t_{1u} and t_{2u} ligand levels are split into a_{2u}, e_u and b_{2u}, e_u couples. For the sake of clarity, the interconnection between the energy levels has been drawn only for the levels derived from the (O_h) t_{2g} and e_g levels, for which the Pt 5d metal character (in percent) is reported in the diagram.

This diagram clearly shows that the levels involving the equatorial chlorine orbitals and the platinum orbitals lying in this plane (d_{xy}, $d_{x^2-y^2}$) remain nearly unchanged. At the same time, the Pt d_{xz}, d_{yz} orbitals, involved in π-type MOs, are very weakly perturbed. In contrast, the energy of the antibonding HOMO is progressively lowered as the Pt–Cl_{ax} bonds are elongated and the energy of the related bonding 5 d_{z^2} MO is increased.

For substantial Pt–Cl_{ax} elongations (e.g. 1 au), the HOMO comes very near to the 5dπ levels while its related bonding partner adjoins the lower π ligand levels. It is thus clear that the LMCT transitions involving the transfer of a ligand electron from the HOMO will be strongly shifted toward the red when the axial Pt–Cl bonds are elongated (see below). In connection with the energy level evolution, it is pertinent to analyze the changes in the Pt and Cl charge distributions, which are presented in Table II and shown in part in Figure 3.

As expected from the preceding remarks, the elongation of the Pt–Cl_{ax} bond lengths involves primarily the electronic populations of the axial chlorines and a smooth evolution in the total Pt charge. The 5dπ Pt charge remains remarkably constant while those of the equatorial chlorines are little altered by the axial deformation. The electronic populations of the Pt 6s, 6p, 5f, and 5dσ orbitals slightly decrease with increasing axial elongation. The $5d_{z^2}$ orbital gains some charge while its $5d_{x^2-y^2}$ partner loses some. Concurrent with the $5d_{z^2}$ charge augmentation is an increase in the Cl_{ax} 3pσ population. This is the principal trend in this evolution: For a standard Pt–Cl elongation of 1 au, the positive net charge of Pt is increased by 0.27 e while each axial chlorine gains 0.24 e.

(25) A. Abragam and B. Bleaney, "Electron Paramaganetic Resonance of Transition Ions", Clarendon Press, Oxford, England, 1970.

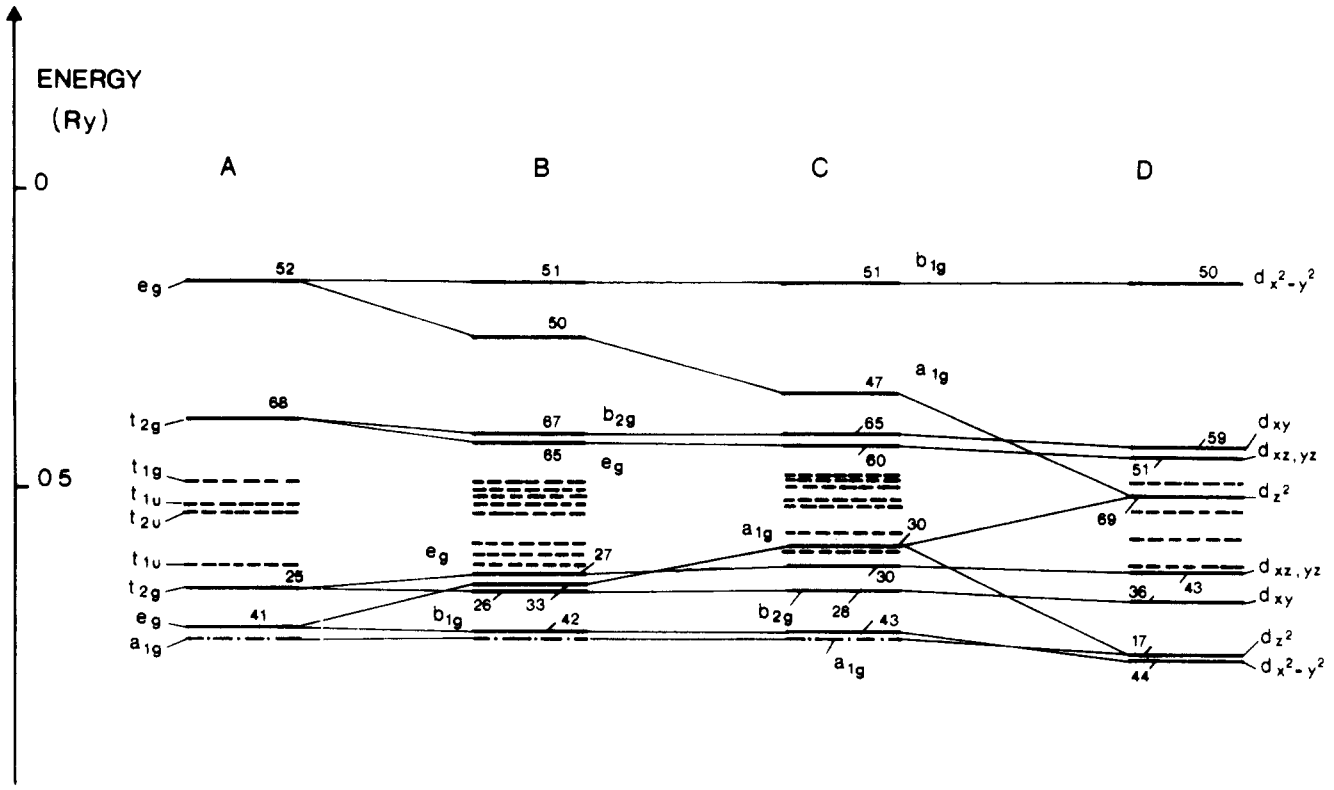

Figure 3. Ground-state valence energy levels of $PtCl_6^{3-}$ without (A) and with $PtCl_{ax}$ bond length elongation (B, 0.4 au; C, 1 au) and of $PtCl_4^-$ (D). The metal contribution in percent is indicated for each level.

Table III. Electronic Energy Levels[a] and Percent Charge Distribution of $PtCl_4^-$

MO	energy, Ry	Pt s	Pt pσ	Pt pπ	Pt d_{z^2}	Pt $d_{x^2-y^2}$	Pt d_{xy}	Pt $d_{xz,yz}$	Pt f	Cl s	Cl pσ	Cl pπ	INT	OUT
$3b_{1g}$	−0.205					50				3	36		8	3
$2b_{2g}$	−0.468						59					31	9	1
$2e_g$	−0.485							51				40	9	
$1a_{2g}$	−0.533											90	9	1
$3a_{1g}$	−0.548	11			69						4		16	
$3e_u$	−0.574		1						1		20	68	10	
$1b_{2u}$	−0.577								1			86	12	1
$1a_{2u}$	−0.618			2								80	17	1
$2e_u$	−0.658		8						1		67	17	5	2
$1e_g$	−0.675							43				44	13	
$1b_{2g}$	−0.728						36					51	13	
$2a_{1g}$	−0.815	13			17					4	64		1	1
$2b_{1g}$	−0.818					44				2	53			1
$1e_u$	−1.467		2						1	94			3	
$1b_{1g}$	−1.474					6				93			1	
$1a_{1g}$	−1.506	4			2					90	1		3	

[a] The highest occupied level is $2b_{2g}$, which accommodates 1 electron.

In this elongated structure, the axial chlorines are thus very similar to formal Cl^- anions since they carry a net negative charge of almost 0.9−. This situation is illustrated in Figure 2C by the plot of the total σ-electronic isodensity contours along the C_4 axis.

This analysis allows us to predict that this model of $Pt^{III}Cl_6^{3-}$ with strongly elongated Pt−Cl_{ax} bond lengths can simulate a predissociation structure leading to $Pt^{III}Cl_4^-$ (or a weakly solvated form of this latter complex at high chloride concentration).

(2) $Pt^{III}Cl_4^-$. The calculated valence levels and corresponding charge distributions of this compound are presented in Table III. With respect to the octahedral structures, the absence of axial ligands leads to substantial changes in the nature and energies of the a_{1g} MOs: a strong mixing occurs between the $2a_{1g}$ and $3a_{1g}$ MOs of the elongated $PtCl_6^{3-}$ structures (originating from Pt 6s−Cl 3pσ and Pt $5d_{z^2}$−Cl 3pσ interactions). The $2a_{1g}$ MO of $PtCl_4^-$ displays some mixed Pt 6s and Pt $5d_{z^2}$ character, but it remains essentially localized in the ligand spheres. At the same time, the $3a_{1g}$ level, which is associated with the antibonding Pt $5d_{z^2}$−Cl 3pσ interactions, becomes more stable than the related π-antibonding $2b_{2g}$ and $2e_g$ MOs. Moreover, its electronic population turns out to be mainly localized in the Pt sphere, changing this MO into a nonbonding one.

The ground state of this square-planar structure is $^2B_{2g}$ since the singly occupied HOMO is now $2b_{2g}$, which corresponds to π-antibonding interactions of the Pt $5d_{xy}$ and Cl 3pπ orbitals. As illustrated by diagrams C and D of Figure 3, the energy levels of $PtCl_4^-$ correlate very well with those of the strongly deformed $PtCl_6^{3-}$ structure. However, some differences in the nature of the HOMO and of ligand MOs will be further pointed out in connection with the interpretation of the absorption spectra.

Table IV. Electronic Energy Levels[a] and Percent Charge Distribution of $PtCl_5^{2-}$ (D_{3h})

MO	energy, Ry	Pt						f	Cl_{eq}			Cl_{ax}			INT	OUT
		s	p_z	p_{xy}	d_{z^2}	$d_{x^2-y^2}$	$d_{xy,yz}$		s	pσ	pπ	s	pσ	pπ		
$5a'_1$	−0.130				50			1	2	12		2	19		9	5
5e′	−0.273			2		54			1	17	13				11	2
3e″	−0.373						66				11			13	9	1
2e″	−0.476										48			41	11	
$3a''_2$	−0.496		1					1			58		29		9	2
4e′	−0.510							1		9	23			56	11	1
$1a'_2$	−0.515							1			86				12	1
3e′	−0.575			3		1				12	38			28	17	1
$2a''_2$	−0.596		7								25	1	58		7	2
1e″	−0.640						26				29			31	13	1
2e′	−0.674			2		36			1	49	10			1		1
$4a'_1$	−0.714	3			36				1	40		1	18			1
$3a'_1$	−0.726	18			4				2	26		2	45		2	1
$2a'_1$	−1.393				5				44			50				1
1e′	−1.394			2		2			94						2	
$1a''_2$	−1.395		2									95			3	
$1a'_1$	−1.437	6							48			43			2	

[a] The highest occupied level is 5e′, which accommodates 3 electrons.

The population analysis leads to the metal and ligand configurations $Pt\{5d^{7.83}[d\sigma^{2.76}(d_{z^2}^{1.76}d_{x^2-y^2}^{1.00})d\pi^{5.07}(d_{xy}^{1.31}d_{xy,yz}^{3.76})]6s^{0.56}6p^{0.48}5f^{0.14}\}Cl\{3s^{1.94}3p\sigma^{1.65}3p\pi^{3.91}\}$.

The calculated Pt net charge (1.0+) is very close to the value obtained for the most elongated $PtCl_6^{3-}$ structure. The main difference between these two Pt^{III} models lies essentially in the populations of the Pt $5d_{z^2}$ and $5d_{xy}$ orbitals. This is easily explained by the stabilization of the former in the planar structure, which implies the redistribution of their electronic populations, according to the Fermi statistics.

(3) $PtCl_5^{2-}$ (D_{3h}). A trigonal-bipyramidal structure is not so easy to correlate with the former postulated models since D_{3h} is not a subgroup of O_h. The calculated electronic structure of $PtCl_5^{2-}$ (D_{3h}) is reported in Table IV.

This structure has a $^2E'$ ground state since the HOMO (occupied by 3 electrons) is 5e′, which corresponds to mixed σ- and π-antibonding interactions between the Pt $5d_{x^2-y^2}$, $5d_{xy}$ orbitals and the 3pσ, 3pπ orbitals of the equatorial ligands. The LUMO $5a_1$ is related to σ-antibonding interactions between the Pt $5d_{z^2}$ and the 3pσ orbitals of all the ligands. The only MO that remains very similar in nature and energy to that of the $PtCl_6^{3-}$ model is 3e″, which provides the π Pt $5d_{xz,yz}$–Cl 3pπ antibonding interactions.

The calculated Pt and Cl configurations are $Pt^{8.92}\{5d^{7.76}(d_{z^2}^{0.90}d_{x^2-y^2,xy}^{3.18}d_{zx,yz}^{3.68})6s^{0.54}6p^{0.54}5f^{0.08}\}Cl_{eq}(3s^{1.94}3p\sigma^{1.71}3p\pi^{3.97})$, $Cl_{ax}(3s^{1.96}3p\sigma^{1.63}3p\pi^{4.00})$.

The ground state of this structure is degenerate; it is thus Jahn–Teller unstable. The rapid conversion from this form to a square-pyramidal structure (C_{4v}), derived from the Berry mechanism,[26] is thus to be expected to split this degeneracy.

Calculated Electronic Transitions of the Transient Models

In the context of this section, it is germane to point out that the experimentally observed transient absorption spectrum consists essentially of one intense band of moderate intensity (see below).

In O_h, D_{4h}, and D_{3h} symmetries, the metal–metal transitions are forbidden by the symmetry selection rules, and if present in the spectra, they will thus correspond to very weak absorption bands. Consequently, it is reasonable to assume that the experimental absorption spectrum manifests primarily the allowed transitions of a charge-transfer type. Since all the transient models have a partially occupied HOMO and a virtual LUMO with preponderant metal characters, the observed transitions in the 230–600-nm range are necessarily ligand to metal charge-transfer (LMCT) transitions. In the following discussion, we will thus only report transitions of this type which are allowed by the symmetry selection rules.

Table V. LMCT Transitions for the Octahedral $PtCl_6^{3-}$ Models (Wavelengths in nm)

transition	nature of the ligand-type MO	elongation of the axial Pt–Cl bonds: 0	0.2 au	0.4 au	1.0 au
$3a_{2u} \rightarrow 5a_{1g}$	Cl_{ax} (3pσ)	212	266	318	540
$4e_u \rightarrow 5a_{1g}$	Cl_{ax} (3pπ)		259	302	477
$3e_u \rightarrow 5a_{1g}$	Cl_{eq} (3pπ)	228	250	276	403
$2e_u \rightarrow 5a_{1g}$	Cl_{eq} (3pσ)	175	203	214	313
$2a_{2u} \rightarrow 5a_{1g}$	Cl_{eq} (3pπ) + Cl_{ax} (3pσ)		207	235	330

Moreover, all the electronic transition energies have been calculated on the assumption that the configurations of the ground state and of the LMCT states are of $(t_{2g})^6(e_g)^2$ types, respectively, without spin–orbit coupling admixtures of $(t_{2g})^5(e_g)^2$ excited (cubic symmetry). Indeed, for the doublet orbital ground state (d^7) as for the singlet orbital LMCT states (d^8), the diagonal elements of the orbital angular momentum are zero and the matrix elements of the metal spin–orbit coupling vanish in the e manifold.

(1) $Pt^{III}Cl_6^{3-}$. The calculated LMCT transitions of $PtCl_6^{3-}$ with various Pt–Cl_{ax} bond lengths are gathered in Table V.

As expected from the diagram of energy levels (Figure 3), the calculated transitions are all shifted toward the red as the Pt–Cl_{ax} bond lengths are elongated. Moreover, the three closely spaced transitions of the O_h model, from $3t_{1u}$, $1t_{2u}$, $2t_{1u}$ to $3e_g$ respectively at 212, 228, and 175 mm) are split into five more separated transitions as the structures become more deformed. Another consequence of the $O_h \rightarrow D_{4h}$ descent in symmetry is to characterize the transition as stemming from the Cl_{ax} or Cl_{eq} ligands, with the movement of electronic charge being from the Cl_{eq} or Cl_{ax} 3pσ and 3pπ orbitals toward the Pt $5d_{z^2}$ orbital.

According to the qualitative rule suggested by Day and Sanders,[27] the only CT transitions that can carry intensity are those having their transition moment polarized in the same direction as the CT itself. In the application of this rule to the present $PtCl_6^{3-}$ case, it follows that only the transitions leading to $^2T_{1u}$ (O_h) and $^2A_{2u}$ (D_{4h}) CT excited states can yield intense absorptions (electrons transferred from the axial

(26) F. A. Cotton and G. W. Wilkinson, "Advanced Inorganic Chemistry", 3rd ed., Interscience, New York, 1972.

(27) P. Day, and N. Sanders, *J. Chem. Soc. A*, 1536 (1967).

Table VI. LMCT Transitions for the $PtCl_5^{2-}$ Model (D_{3h})

transitions	nature of the ligand-type MO	wavelengths, nm
$1e'' \rightarrow 5e'$	Cl_{eq} (3pπ) + Cl_{ax} (3pπ)	228
$3a''_2 \rightarrow 5a'_1$	Cl_{eq} (3pπ) + Cl_{ax} (3pσ)	232
$3e' \rightarrow 5e'$	Cl_{eq} (3pπ) + Cl_{ax} (3pπ)	264
$4e' \rightarrow 5e'$	Cl_{eq} (3pπ) + Cl_{ax} (3pπ)	323
$1a'_2 \rightarrow 5e'$	Cl_{eq} (3pπ)	329
$2e'' \rightarrow 5e'$	Cl_{eq} (3pπ) + Cl_{ax} (3pπ)	374

chlorines to Pt along the z axis for the elongated structures).

We therefore conclude that the $3a_{2u} \rightarrow 5a_{1g}$ and $2a_{2u} \rightarrow 5a_{1g}$ transitions, involving a CT from the Cl_{ax} 3pσ to Pt $5d_{z^2}$ orbitals, must be related to intense absorption bands. All the other transitions are expected to be weak. The intense absorptions are calculated at 212 and 175 nm for the regular octahedral $PtCl_6^{3-}$ complex and at 540 and 330 nm for the most elongated structure.

Nevertheless, we must stress the fact that the overlap between metal and axial ligand orbitals is necessarily smaller for the most elongated structure, involving a somewhat decreased intensity for these transitions.

(2) $PtCl_4^-$ (D_{4h}). From the diagram of Figure 3D, it is obvious that only two LMCT transitions are possible for this Pt(III) model. The $2e_u \rightarrow 2b_{2g}$ and $3e_u \rightarrow 2b_{2g}$ allowed transitions are calculated repectively at 410 and 620 nm.

The $2e_u$ and $3e_u$ ligand levels have mixed Cl 3pσ and Cl 3pπ characters, predominantly Cl 3pσ for the former and Cl 3pπ for the latter. The final $2b_{2g}$ level having a Pt $5d_{xy}$ character, the LMCT transitions involve primarily orbitals within the molecular plane.

According to the aforementioned rule, these transitions are expected to be related to intense absorption bands, since they lead to ^2E_u excited states, polarized in the molecular plane.

As is expected for these kinds of transitions, the associated absorption bands will likely exhibit substantial intensity, probably comparable to that of related LMCT transitions of various d^4 and d^5 complexes.[23] For example, in the $IrCl_6^-$ complex,[25] the LMCT transitions from mixed Cl 3pσ and Cl 3pπ ligand MOs to the Ir 5dπ orbital correspond to absorption bands in the 400–500-nm region with ϵ values of about 2500–3000 M^{-1} cm^{-1}, whereas the LMCT transitions from the same ligand levels to the Ir 5dσ (d_{z^2}, $d_{x^2-y^2}$) level are assigned to an absorption band with an ϵ value of about 20000 M^{-1} cm^{-1} at 262 nm.

(3) $PtCl_5^{2-}$ (D_{3h} and C_{4v}). The calculated LMCT transitions of the D_{3h} transient model are presented in Table VI.

All of these allowed transitions, but one, correspond to the transfer of a ligand electron to the 5e′ HOMO (Pt $5d_{xy}$, $5d_{x^2-y^2}$). The only allowed LMCT transition to the $5a'_1$ LUMO (above 200 nm) is $3a''_2$ electron $\rightarrow$ $5a'_1$. For this structure, the CT occurs in the equatorial plane. The transitions leading to the $^2E'$ excited states can thus yield intense absorption bands. They are calculated at 264, 323, and 329 nm.

In fact, the D_{3h} arrangement of the three equatorial ligands does not favor the overlap of their 3pπ orbitals with the Pt $5d_{xy}$, $5d_{x^2-y^2}$ orbitals. In addition, these Pt orbitals have a quite small overlap with the parallel 3pπ orbitals of the axial chlorines.

The calculated LMCT transitions for the C_{4v} form with and without elongation of the Pt–Cl_{ax} bond will be presented elsewhere.[17] The corresponding CT transitions that could yield intense absorption bands must generate $^2A_1$ excited states (electrons transferred along the z axis). They are gathered in Table VII.

Comparison with Experiment

The reaction of e_{aq}^- with $Pt^{IV}Cl_6^{2-}$ [11a] and the flash photolysis[10c] of this compound yield the same species, absorbing at 410 nm (ϵ = 3700) and attributed to a Pt(III) transient. In the first experiment, a primary product could be generated but its absorption spectrum is not produced. In the flash photolysis experiment, the product absorbing at 410 nm is the unique species. It results from the transfer of an electron from a pure ligand MO of $PtCl_6^{2-}$ to the $3e_g$ 5dσ MO,[16] induced by light absorption at the wavelengths of the charge-transfer band of this complex (λ_{max} = 262 nm, ϵ = 24500 M^{-1} cm^{-1}). This intramolecular electron transfer reaction produces a d^7 ($t_{2g}^6e_g$) complex, very similar to $Pt^{III}Cl_6^{3-}$, as described in the present work.

In a previous paper, one of us[7a] suggested that, beyond the classical direct photochemical homolysis scheme, another one, more indirect, could play a nonnegligible role, under favorable circumstances. In the direct photochemical scheme, the photon induces the transition of an electron toward an antibonding orbital, weakening therefore the overall bond. In the indirect photochemical homolysis scheme, the main role of the photon is to create a highly oxidizing excited state: this excited state is therefore in a good situation to accept an electron from the medium, and it is mainly this addition of electron that eventually leads to rupture. The preceding paragraph shows that, for $Pt^{IV}Cl_6^{2-}$ itself,[6] the direct photochemical homolytic scheme has good chances to occur. We have seen indeed that the LMCT transition not only transfers one electron in an e_g antibonding orbital but furthermore creates a hole mainly located in a nonbonding orbital. The MS-Xα calculated electronic structure of this LMCT excited state indicates that no modification occurs in the bonding and antibonding metal–ligand interactions. Furthermore, the metal charge is not modified and the hole remains fully localized on the ligands. Therefore, it is likely that, even if the excited state were to accept an electron from the medium, it would populate ligand MOs, resulting in only small modifications to the Pt–Cl bonds. If indirect homolysis (Scheme II) were to play a photochemical role in Pt^{IV} complexes, it would probably be when the ligands are such that the overall complex bears a positive charge.[4c,10b] However, Shagisultanova[28] reports the experimental results for photochemically induced electron transfer from SO_4^{2-}, Cl^-, Br^-, or I^- to increase along the series $PtCl_6^{2-}$ < $PtBr_6^{2-}$ < $Pt(en)_3^{4+}$ < $Pt(NH_3)_5I^{3+}$ < $Pt(NH_3)_4I_2^{2+}$ < PtI_6^{2-} < $Pt(Glyc)_3^+$. More experimental and theoretical work is needed to settle the issue of direct vs. indirect homolysis in Pt complexes, but it seems that, for $PtCl_6^{2-}$, the former[6] dominates.

The situation in regard to the metal–ligand σ bonding is illustrated in Figure 2. From this, it is reasonable to assume that flash photolysis leads to the deformation of the initial $PtCl_6$ regular octahedron and, then, to the breaking of metal–ligand bonds.

The final product presents a unique band (ϵ = 3700) in the region 350–500 nm. Unfortunately, we do not have experimental spectra in the 250–350- and/or 500–650-nm regions. In the pulse radiolysis study, the explored wavelength ranges are similar. The experimentally investigated region is thus quite narrow to compare efficiently with the calculated LMCT spectra of the transient models.

We have gathered in table VII the calculated LMCT transitions of each studied structure, including the C_{4v} models, which are expected to have substantial intensities, according to the qualitative rule of Day and Sanders.

Examination of Table VII leads to the first conclusion that the $PtCl_5^{2-}$ D_{3h} structure has no calculated transition expected to be intense in the 350–500-nm region. Moreover, owing to

(28) G. A. Shagisultanova, A. A. Karahan, and A. L. Pozuyak, *Khim. Vys. Energ.*, **5**, 368 (1971); *High Energy Chem. (Engl. Transl.)*, **5**, 333 (1971).
(29) C. K. Jørgensen, "Absorption Spectra and Chemical Bonding in Complexes", 2nd ed., Pergamon Press, Elmsford, NY, 1964.

Table VII. Calculated LMCT Transitions of Chloro Pt(III) Complexes That Are Assumed To Be Intense

	$PtCl_6^{3-}$				$PtCl_5^{2-}$ (D_{3h})	$PtCl_5^{2-}$ (C_{4v})			$PtCl_4^-$	exptl range (350–500 nm)
elongation of the axial Pt–Cl bond, au	0	0.2	0.4	1.0	0	0	0.4	1.0		Pt(III) species
wavelengths, nm	212	266	318	540	264 323			560	620	
	175	207	235	330	329	206	270	448	410	410 (ϵ = 3700)

the ground-state unstability of the D_{3h} structure, it cannot be related to a long-lived transient, as that observed at 410 nm.

It thus seems reasonable to eliminate from consideration, for the observed Pt(III) transient, a D_{3h} $PtCl_5^{2-}$ structure as originally proposed by Adams and co-workers.[11a] Similarly, the $PtCl_6^{3-}$ and C_{4v} $PtCl_5^{2-}$ models, without or with moderate bond length elongation (≤0.4 au), can also be ruled out since their CT absorption bands are located at too high energies (≤330 nm). All these structures, derived from cubic symmetry, are expected to provide ligand pσ to metal dσ CT transitions related to very intense absorption bands ($\epsilon \simeq 20000$ M^{-1} cm^{-1}).

At this stage in our discussion it is worthwhile to point out that such strongly absorbing transients, in the 230–300-nm region, have been detected in pulse radiolysis studies of reactions from $Pt(en)_2X_2^{2+}$ (X = OH, Cl).[30] These spectral properties were then attributed to "product structures being basically distorted octahedra with the possible limiting forms of square pyramidal or square planar". On the basis of the present study, we can now be somewhat more precise in that the square-planar structure can be eliminated (even with two labile substituents in the fifth and/or sixth coordination site) because strong absorption bands in the 230–300-nm region are necessarily related to only small axial elongations (≤0.2 Å) of the octahedral or square-pyramidal forms.

Three models, among the calculated ones, could correspond to the observed transient. In fact, they are all derived from the same structure, that is a square-planar $PtCl_4^-$ complex, with eventually one or two loosely bonded chloro ligand(s).

The presence of one apical chlorine ($PtCl_5^{2-}$), at about 2.85 Å from Pt, does not change substantially the CT spectrum with respect to $PtCl_4^-$. For both these structures, there must be another absorption band besides the observed 410-nm one, near 530 nm for $PtCl_5^{2-}$ or 620 nm for $PtCl_4^-$, that is out of the experimentally observed range. If one considers an hexacoordinated structure, the 410-nm absorption band is consistent with two elongated Pt–Cl_{ax} bonds of about 2.70 Å (value obtained by interpolation of the results at various elongations). In that case, another absorption band is expected near 280 nm, which is quasi-superposed with the CT spectrum of the original $PtCl_6^{2-}$ product.

In summary, our results serve to more clearly delineate the possible structures for platinum(III) chloro systems, and in particular they indicate that the trigonal-bipyramidal $PtCl_5^{2-}$ is not to be favored. Furthermore, the comparison between theory and experiment points to the transient being distorted from strict O_h symmetry, in a manner generally consistent with an earlier proposal.[10c] For the forms with apical chloro ligand(s), the distance between the metal center and apical substituent must be substantially larger than the more usual Pt–Cl bond lengths (at least 0.5 Å). Each of these structures as well as that for square-planar $PtCl_4^-$ are predicted to have an absorption band of substantial intensity near that observed at 410 nm. More extensive spectral information, which we are in the process of obtaining, is needed before one can make a more concrete choice between the possible options.

Acknowledgment. The financial support of NATO (Project No. 010-81) and the Natural Sciences and Engineering Research Council of Canada are gratefully acknowledged. Part of the calculations have been performed at the "Centre de Calcul CNRS" of Strasbourg-Cronenbourg.

Registry No. $PtCl_6^{2-}$, 16871-54-8; $PtCl_6^{3-}$, 50790-36-8; $PtCl_5^{2-}$, 34076-49-8; $PtCl_4^-$, 92011-15-9.

(30) (a) J. C. Brodovitch, D. K. Storer, W. L. Waltz, and R. L. Eager, *Int. J. Radiat. Phys. Chem.*, **8**, 465 (1976); (b) W. L. Waltz, J. Lilie, R. T. Walters, and R. J. Woods, *Inorg. Chem.*, **19**, 3284 (1980).